Journal of Nuclear Materials 389 (2009) 470–478

Contents lists available at ScienceDirect

Journal of Nuclear Materials

journal homepage: www.elsevier.com/locate/jnucmat

Reaction of neptunium with molecular and atomic oxygen: Formation and stability of surface oxides

A. Seibert *, T. Gouder, F. Huber

European Commission, JRC, Institute for Transuranium Elements (ITU), Postfach 2340, 76125 Karlsruhe, Germany

ARTICLE INFO

Article history:
Received 13 January 2009
Accepted 2 March 2009

ABSTRACT

The surface reactions of thin films of Np metal with molecular and atomic oxygen were investigated by X-ray and Ultra-Violet Photoelectron Spectroscopy (XPS and UPS, respectively). Goal of this work was to study the entire range of oxides, starting with the very early reaction stages, in presence of metal, up to the highest possible oxides, reached at saturation under highly reactive, oxidative conditions. Emphasis was given to the surface layers, whose properties often differ from the bulk, and which are directly involved in corrosion processes of solids. Molecular O_2 reacts readily with the metallic neptunium surface to form the sesquioxide and dioxide. The sesquioxide is observed as thin 'bulk' species of up to nine monolayers thickness. A higher oxide, identified as Np_2O_5, is formed when the NpO_2 surface is exposed to atomic oxygen. It is stable under UHV conditions up to a temperature of about 200 °C. The high oxide, Np_2O_5, is still capable of chemisorbing further oxygen. This is shown in UPS spectra by the additional O-2p line at 5–6 eV BE, superimposing onto the valence band (VB). The formation of both a lower (Np_2O_3) and higher oxide (Np_2O_5) besides the dioxide is discussed in the framework of ongoing 5f localization throughout the actinide series.

1. Introduction

Actinide dioxides AnO_2 are commonly used as conventional and advanced reactor fuel types (An = Th, U, Pu) or build up as minor actinides during in-reactor irradiation (An = Np, Am, Cm). The long term chemical stability of these oxidic fuels plays an important role in the performance assessment of potential nuclear waste disposal concepts [1]. One particularly important scenario is the dissolution of fuel once in contact with groundwater. The possible formation of higher actinide oxides out of the dioxides (UO_2 and PuO_2 or the mixed oxide matrices) directly influences the dissolution behaviour of the spent fuel, because the solubility of the actinide oxides increases drastically when the actinide has an oxidation state above +4 [2]. The claimed existence of PuO_{2+x} (s) [3,4] – after decades of believing in a very stable PuO_2 – and the controversial discussion following this surprising statement [5–7] unveiled the fact that especially for plutonium, as well as neptunium, the existing data set concerning their An–O phase diagrams is unsatisfactory [8].

In an earlier publication we focussed on the surface reactions of Pu with molecular (O_2) and highly reactive atomic oxygen (O·) [9]. To situate the oxidation behaviour of Pu amongst the actinide series, we did a systematic comparison of the Pu and U reactions over the entire oxidation range, starting with the metal surfaces and ending with the highest stable oxide. To complete this series it is interesting to render similar information about the oxidation behaviour of the intermediate actinide, i.e. neptunium.

UO_2 and PuO_2 both form spontaneously when the metal surfaces are exposed to molecular oxygen [9,10]. Low rates of 10–20 Langmuirs (Langmuir, 1 L = 1.33×10^{-4} Pa s, i.e. the dosage needed to cover one monolayer if all gas atoms stick to the surface) are sufficient to form several monolayers of the dioxide. Transient Pu_2O_3, which is found in the earlier stage of oxidation, is rapidly transformed into PuO_2 at these dosages [11]. At the AnO_2 stage, the oxidation slows down. The dioxide surfaces have only a small affinity for O_2 – much smaller than the metal – which is explained by the difficulty of molecular oxygen to adsorb and dissociate on them, before incorporating into the lattice sites. If O_2 dissociation is indeed the rate limiting step in the oxidation process, then further oxidation should occur readily in presence of atomic (i.e. pre-dissociated) oxygen. The experiment showed indeed [9] that atomic oxygen readily reacts both with UO_2 and PuO_2 surface layers at room temperature, forming UO_3 and PuO_{2+x}. At elevated temperature, when bulk diffusion becomes allowed, even bulk UO_2 is oxidised to bulk UO_3 under saturation conditions. Bulk PuO_2, on the other hand, does not oxidize but instead the higher surface oxide decomposes releasing oxygen into the gas phase. This behaviour reflects the difference in stability of higher oxides of uranium and plutonium. It can be related ultimately to the increasing contraction of the 5f states with increasing nuclear charge (5f trend towards localisation) leading to a lowered 5f bonding tendency in Pu than in U [12]: uranium forms a wide variety of stable bulk binary oxides ranging from

* Corresponding author. Tel.: +49 0 7247 951234.
E-mail address: alice.seibert@ec.europa.eu (A. Seibert).

0022-3115/$ - see front matter © 2009 Elsevier B.V. All rights reserved.
doi:10.1016/j.jnucmat.2009.03.002

UO_2 up to UO_3 with various intermediate phases. For the higher actinides neptunium and plutonium the variety of binary oxide compounds is drastically decreased, despite the fact that these elements show a wide range of oxidation states in solution, oxidation states III–VI for Pu and III–VII for Np are described [8]. Based on the bulk compound data, two anhydrous oxides, NpO_2 and Np_2O_5, as well as some hypostoichiometric phases exist, as shown by the Np–O phase diagram [8]. The higher oxide $NpO_{2.6}$ claimed in early reports (produced by several methods), was shown later, during the 70s, to be most likely Np_2O_5 [8]. Exposure of dry neptunium(V) hydroxides to atomic oxygen, which oxidised U_3O_8 readily to UO_3 at temperatures >200 °C, gave no clear evidence for higher neptunium oxides (with Np(VI)) [13]. Hydrous trioxides ($AnO_3 \cdot yH_2O$) are reported for uranium as well as plutonium and neptunium [8].

In this paper we will describe the surface oxidation of Np metal films first exposed to molecular then to atomic oxygen, to cover the entire range from low to high surface oxidation states. The photoemission data from XPS and especially the valence band spectra obtained from UPS provide information on the electronic structure of the systems, thereby contributing to a deeper understanding of the complex corrosion behaviour of actinide oxides.

2. Experimental

Neptunium metal films were prepared by direct-current (DC) sputter deposition from a neptunium metal target with Ar as sputter gas. Films were deposited on silicon wafer plates (1 1 1), cleaned in situ by argon ion sputtering before the deposition. The plasma in the diode source was maintained by injection of electrons of 50–100 eV energy. This allowed operating at a relatively low sputter gas pressure below 1 Pa. The background pressures in the preparation and in the analysis chamber were around 3×10^{-7} Pa or better. The neptunium target consisted of a neptunium metal rod (10 mm length, 2 mm diam.). Ultrahigh purity Argon (99.9999%) was used for all experiments. Oxygen used as reactive gas was 99.9999% grade. Atomic oxygen was produced by an electron cyclotron resonance (ECR) Plasma Source Gen I from Tectra GmbH, Frankfurt/M. The atom flux is specified to $>10^{16}$ atoms/cm^2/s, corresponding to an exposure of roughly 10 Langmuir/s (i.e. 10^{-3} Pa O).

XPS and UPS spectra were recorded using a Leyboldt EA-10 hemispherical analyzer. Mg K_α (1253.6 eV) excitation radiation was used for the XPS experiments. UPS spectra were taken with HeI (21.22 eV) and HeII (40.81 eV) UV light, produced by a high intensity windowless discharge lamp. Taking advantage of the different mean free paths (λ) for HeI, HeII and Mg K_α excited photoelectrons, bulk and surface properties have been accessed [14]. In addition, the energy dependent photoionisation cross-sections [15] allowed identification of the orbital character (p, d or f) of the valence band region. A summary of the characteristics of the excitation radiation is given in Table 1.

3. Results and discussion

3.1. Reaction of Np metal with molecular oxygen

3.1.1. Valence band data

Fig. 1 shows the UPS valence band (A) and XPS 4f core level (B) spectra of a deposited neptunium metal film exposed to different dosages of molecular oxygen.

Table 1
Characteristics of the excitation radiation used.

Radiation in eV	Probed electron energy level	Photoionisation cross-section in Mbarn [15]	Mean free path, λ, in monolayers [14]
HeI, 21.22	Valence band (Np-5f, O-2p)	0.7113 (Np-5f) 10.67 (O-2p)	2–4
HeII, 40.81	Valence band (Np-5f, O-2p)	6.266 (Np-5f) 6.816 (O-2p)	1–2
Mg K_α, 1253.6	Np-4f	1.188	6–8
Mg K_α, 1253.6	O-1s	0.063	6–8

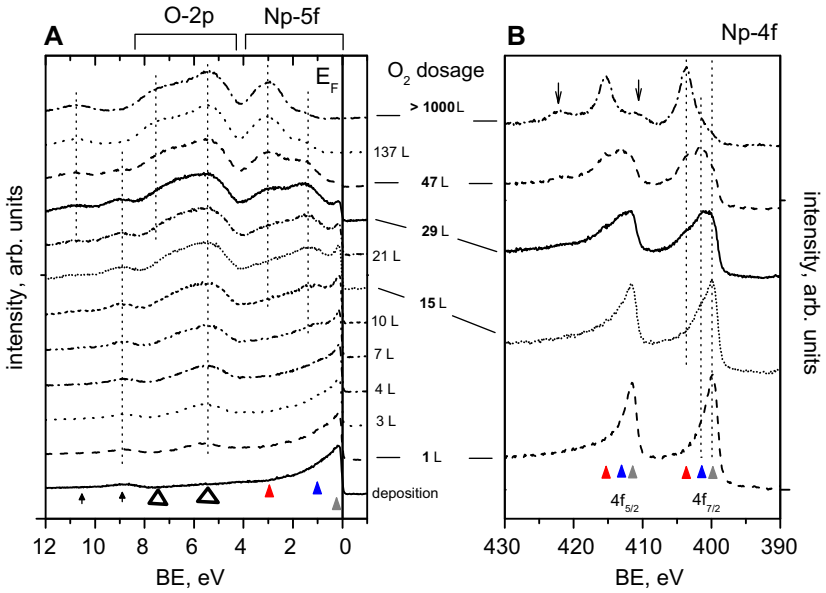

Fig. 1. UPS valence band (A) and XPS Np-4f core level (B) spectra of a deposited Np metal film exposed to different dosages of molecular oxygen (1 L to about 1000 L). Bold typed dosage values are valid for figure A and B. The solid line in A represents the Fermi energy, E_F. The different species of Np (metal, sesquioxide, dioxide) are marked with filled symbols (grey squares, blue triangles, red points). Open triangles in A are indicating O-2p features. Arrow marks are explained in the text. For UPS HeII radiation (40.8 eV) and for XPS Mg K_α excitation radiation (1253.6 eV) was used. No change in BE or FWHM for O-1s is observed (not shown). (For interpretation of the references to colour in this figure legend, the reader is referred to the web version of this article.).

The initial neptunium film (Fig. 1(A), lowest spectrum) shows the typical Np metal spectrum with the maximum intensity at the Fermi level (marked by the filled square) and a featureless tailing to higher binding energy (BE). The maximum at the Fermi level (0 eV BE) is attributed to the conduction band dominated by itinerant, i.e. bonding, 5f states. The long tail to higher BE is due to the inelastic background, the unresolved Np-6d7s emission and the intrinsic asymmetry of photoemission peaks in systems with a high density of states (DOS) at the Fermi-level [16,17]. After exposure to ~1 L O_2 a peak grows at 5.6 eV binding energy (marked with an open triangle in Fig. 1(A)). It is attributed to the O-2p signal of surface oxygen. Its narrow and symmetrical shape is typical for isolated, chemisorbed oxygen atoms forming local bonds instead of the broad valence band of a bulk oxide [18,19]. Up to dosages of ~3 L the O-2p peak retains its symmetrical shape. The Np-5f level does not change significantly except for a slight decrease in intensity – which may be attributed to the presence of an oxygen overlayer attenuating the signal of the underlying metal. For higher O_2 dosages the O-2p peak broadens into an asymmetrical peak with a maximum at 5.6 eV and a distinct contribution at higher BE (~7.5 eV, second open triangle in Fig. 1(A)), showing the isolated level transforming into the solid state band of a bulk compound [20]. Two supplementary peaks appear with increased oxygen exposure, at 1.3 and 3.0 eV binding energy, respectively. Both peaks are attributed to Np-5f states, because they are suppressed in HeI excited spectra, which is typical for f-states due to their lower cross-sections for HeI radiation (see Table 1 [15]). The peak at 1.3 eV BE appears at intermediate dosages (10–50 L). It is the dominant species around 20 L, but then strongly decreases at higher dosages (137 L). It is incrementally substituted by the peak at 3 eV BE which appears from ~29 L on. These peaks were previously observed for Np metal surfaces, slowly oxidized by surface diffusion of a bulk oxygen contamination [20]. The 1.3 eV peak (marked with the filled triangle Fig. 1(A)) is attributed to the localized $5f^4$ level of Np_2O_3, while the 3 eV peak (marked with the filled point) is due to the $5f^3$ level in NpO_2. Np_2O_3 (sesquioxide) is a transient species which seems to be stable only in the presence of the metal. This behaviour is consistent with the position of Np between Pu, which is the first actinide showing a stable bulk sesquioxide, and U, where no sesquioxide is observed. We relate the increasing stability of this trivalent state to the 5f localization with increasing nuclear charge *Z* (atomic number) [12]. This gives the later actinides their rare-earth like properties, where the valence is determined by the $(6d7s)^3$ configuration. For Np the sesquioxide is still observed, but it is confined to the surface region. This is explained by the additional tendency for 5f localization at the surface [9], because of the lowered coordination. An estimation of the layer thickness of the sesquioxide is given in Section 3.1.2.1 on the basis of the core level data.

Two additional weak features are observed at 9 and 10.8 eV (Fig. 1(A), small arrows). Their origin is speculative. Similar features were observed previously on Pu oxide and U oxide [17] bulk compounds, and were attributed to defects in the oxide lattice. But there are also thin film data for An oxides, which do not show this feature [9,17] indicating that this peak is indeed not intrinsic to the oxides. The possibility of a contamination (bulk or surface) can not be excluded: OH surface species, originating from the chamber walls could explain this signal. In some cases, a fluorine contamination was observed by core level spectroscopy, which would also contribute to this signal.

3.1.2. Core level data

Fig. 1(B) shows a selection of the corresponding Np-4f core level spectra for different O_2 exposures of a metallic neptunium surface. The first spectrum shows the typical metal spectrum, with the spin-orbit split levels at 400.1 eV BE ($4f_{7/2}$) and 411.8 eV BE ($4f_{5/2}$) (marked with the set of filled squares, grey). The asymmetry of the peaks is related to the high density of states (DOS) at the Fermi-level in Np metal (Fig. 1(A)). With increasing oxygen dosage the same behaviour as for the valence band is observed. Starting with an oxygen dosage of 10 L (spectrum not shown in Fig. 1(B)) a peak appears at 1.5 eV higher BE than the metal line (marked with a set of filled triangles, blue). This peak is attributed to the sesquioxide (Np_2O_3). At low dosage, the Np_2O_3 signal is less pronounced in the Np-4f line than in the VB spectra. This is due to the different surface sensitivities (Table 1) of the two excitation radiations. Because the Np_2O_3 species is confined to the outer surface layer, it is intense in the surface selective UPS spectra, but for the 'deeper' looking XPS, the remaining metal atoms from the deeper layers still dominate at this early stage of oxidation. At ~50 L O_2 the Np_2O_3 signal becomes dominant but then decreases in favour of a species with a BE ~3.7 eV higher than the metal species (set of filled points, red). This species is attributed to NpO_2 in presence of Np_2O_3 and Np metal. The binding energy differences between metal, sesquioxide and dioxide are similar for 4f and 5f peaks (see Table 2). They agree well with the chemical shift expected for higher oxidation states, which is mainly explained by the larger ionization potential for the different cations (and therewith an increase of the orbital energy) [21,22].

The Np-4f core level spectrum of NpO_2 shows an intense satellite at ~7 eV higher BE than the main peaks ($4f_{7/2}$ and $4f_{5/2}$), marked with arrows in Fig. 1(B) (uppermost spectrum). Similar satellites are also observed for other actinide dioxides with CaF_2 structure, ThO_2, UO_2, PuO_2 and AmO_2 [23]. They are conspicuous and their origin has been discussed in various theoretical frameworks. They have been attributed to interatomic shake-up effects accompanying the photoemission process. Transition from O-2p (VB) to unoccupied An-5f or -6d states [24–28] has been proposed. Recently the charge transfer nature of the satellite was further verified [29]. In alternative assignments, the satellites were explained by a shake down process from 6d or 5f [30] screening orbitals (reverting the assignment of main peak and satellite peak), or interpreted in the framework of the Anderson impurity model [31], where the energy splitting between satellite and main line is discussed in terms of O-2p/An-5f hybridisation. So, even though the final explanation of this feature is not settled, it is a robust intrinsic signature of NpO_2, used throughout this paper to confirm its presence.

3.1.2.1. Oxide layer thickness from core level spectra (Np-4f).

Both in XPS (Np-4f) and in UPS (valence band) it is not possible to obtain a pure sesquioxide spectrum. This proves well the transient character of Np_2O_3, which is not reported as single bulk phase.

Table 2
Binding energies in eV of Np-5f, Np-4f and O-1s peaks. Charge referencing to C-1s is not possible, therefore O-1s level is given as reference level showing that no drastic charging takes place (the insulating films are too thin)[c]. For the spin orbit split Np-4f level only the value for the $4f_{7/2}$ peak is given. For the low oxides series the BE for Np, Np_2O_3 and NpO_2 are invariable (<0.1 eV) throughout the series, therefore no error estimate (standard deviation) is given.

	BE in eV		
	Np-5f	Np-$4f_{7/2}$	O-1s
Metal	0	400.1	–
Np_2O_3	1.3	401.6	530.8
NpO_2 (+Np_2O_3)	3.0	403.8	530.8
NpO_2[a]	2.0 ± 0.2[c]	402.9 ± 0.2[c]	530.0 ± 0.3[c]
Np_2O_5[b]	1.7 ± 0.2[c]	402.9 ± 0.3[c]	529.6 ± 0.3[c]

[a] Values from [35] 5f: 2.4 eV, $4f_{7/2}$: 403.1 eV.
[b] Values from [35] 5f: 2.2 eV, $4f_{7/2}$: 403.1 eV.
[c] Variations are possible from specimen to specimen, this is thought to be due to slight charging effects (as the differences were similar for the different levels, in the case all levels were measured).

Knowledge of the layer thickness allows to decide, whether Np_2O_3 is only a top surface species (associated with 2D character) or whether it still forms as a, even though thin, bulk phase. The thickness is obtained from the measured Np-4f intensities (i_{Np}, i_{NpO_2}, $i_{Np_2O_3}$, peak areas from subtraction process corrected with Shirley background) of the Np, Np_2O_3, NpO_2 species. The three strongly overlapping components were separated by subtraction technique. First, the metal contribution is isolated by subtracting a Np metal reference spectrum. Then the NpO_2 contribution is determined by subtracting a NpO_2 reference spectrum leaving the Np_2O_3 spectrum. In Fig. 2 these relative intensities are plotted versus the O_2 dosage. The metal signal decreases rapidly at low dosages then the intensity decrease slows down. This is attributed to the migration of the reaction front out of the region probed by XPS, so that the oxidation of lower layers is no longer detected. It may also be due to the slowing down of oxidation when oxygen has to diffuse through thicker oxide layers [10]. Both Np_2O_3 and NpO_2 grow from low dosages on, as seen by the simultaneous growth of the two oxide lines. Around 60 L, the Np_2O_3 signal goes though a maximum then decreases again, showing the sesquioxide to be replaced by the dioxide. To obtain an estimation of the layer thickness, a simple intensity analysis, based on the signal attenuation by overlayers was performed. In general, when a substrate is covered by a continuous overlayer and when a layered growth is assumed, the signals of the covered substrate (i_S) and the overlayer (i_A) are related to the overlayer thickness (d_A) by the following Eqs. (1) and (2) [32]:

$$i_S = i_S^{\infty} \cdot \left(e^{-\frac{d_A}{\lambda_A}} \right), \tag{1}$$

$$i_A = i_A^{\infty} \cdot \left(1 - e^{-\frac{d_A}{\lambda_A}} \right), \tag{2}$$

i_S^{∞}: signal of the uncovered substrate; i_A^{∞} is the intensity of overlayer material of bulk thickness; λ_α the inelastic mean free path.

In our experiments, three layers are considered (Fig. 3), the underlying metal, the intermediate Np_2O_3 (of thickness d_2) and the superficial NpO_2 layer (of thickness d_1). The same λ is assumed for all three layers (λ = 8 ML). This value is obtained from general tabulation [14]. For all three materials the same i^{∞} is assumed ($i_{Np}^{\infty} = i_{Np_2O_3}^{\infty} = i_{NpO_2}^{\infty}$). This is an approximation because the three materials differ in density and composition, but still valid because the atomic cross-sections of the core-level lines are unchanged. Applying Eq. (1), the Np-4f metal signal (i_{Np}) yields the total overlayer thickness, d_3 (= d_1 + d_2) (Fig. 3, Eq. 1b). Applying Eq. (2), the NpO_2 intensity (i_{NpO2}) yields the NpO_2 overlayer thickness (d_1) (Fig. 3, Eq. 1a). d_2 is obtained by simple subtraction. The layer thicknesses, d_n, are directly proportional to λ as seen from Fig. 3, Eqs. (3) and (4). The so obtained layer thicknesses of Np_2O_3 and NpO_2 are plotted as function of O_2 dosage in Fig. 4. This is only a rough estimate, but it allows a number of conclusions to be drawn. The Np_2O_3 layer is clearly thicker than one monolayer. It is not just a top-surface layer or 2D layer but represents a true, even though

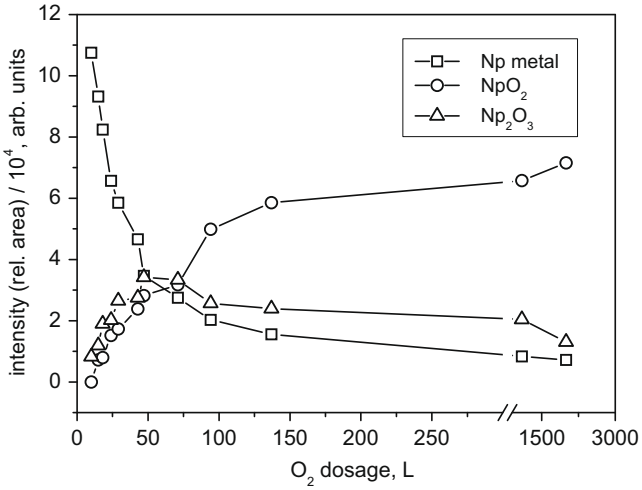

Fig. 2. Evolution of intensities (relative areas of the Np-4f$_{7/2,\ 5/2}$ peaks) for the different Np species as a function of O_2 dosage: Np metal (squares), Np_2O_3 (triangles) and NpO_2 (circles).

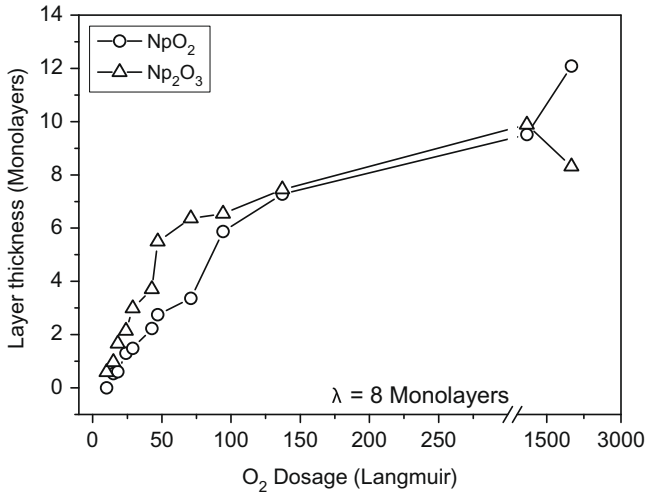

Fig. 4. Estimated thicknesses of the neptunium oxide layers (Np_2O_3, triangles and NpO_2, circles) on neptunium metal as function of the O_2 dosage.

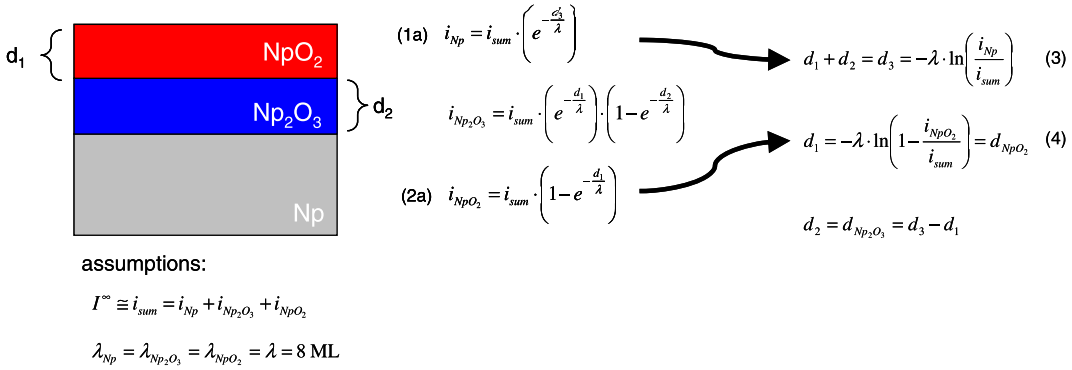

Fig. 3. Method for layer thickness calculation.

thin, bulk compound. Nevertheless, the layer thickness saturates at a value of roughly nine monolayers, while the NpO_2 layer continues to grow. In the layered model it is assumed that the sesquioxide exists as a zone of constant thickness between the underlying metal and the NpO_2, which is the final, stable oxide. This is a simplification, because sesquioxide and dioxide co-exist over the entire dosage range as shown by Fig. 4.

We conclude that the sesquioxide appears as transient (bulk) species of several MLs thickness. Its stability is correlated to 5f localization triggered by the increased nuclear potential, Z_{eff}. This localisation is expected to be more pronounced at the surface, because of 5f band narrowing (due to lowered coordination). Therefore it is not surprising, that the trivalent character in the actinides series first appears in the surface layers as transient oxide in neptunium and becomes more pronounced in the following elements of the series showing increasingly stable bulk sesquioxides [8].

3.2. Reaction of NpO_2 with atomic oxygen

3.2.1. Valence band data

To test for the possible formation of higher oxides, NpO_2 films were exposed to atomic oxygen, produced by dissociating O_2 in an ECR plasma source. Initial exposures were done at room temperature. Fig. 5 summarizes the UPS spectra for successive O· dosages. The initial NpO_2 film (Fig. 5, a) was prepared by exposing a Np metal film to a saturation dose of O_2 (~300 L). The first exposure of this film to atomic oxygen (around 6×10^{17} atoms/cm^2, corresponding to 600 L, as calculated from the specifications of the atom source) results in a shift of the Np-5f and O-2p valence levels to 0.7 eV lower BE (Fig. 5(A), b). This rigid, coherent shift to lower BE is generally considered as a characteristic for the decrease of the Fermi energy in the surface layers probed. Since the photoemission lines of conducting solids are referenced towards the Fermi energy (the electrochemical potential), a decrease of the Fermi energy, i.e. shift towards the occupied levels, is detected as a coherent shift of all electronic levels towards the Fermi level, i.e. to lower BE. In the present case, the Fermi energy shift can be attributed to the formation of a dipole layer formed by chemisorbed atomic oxygen, building up a dipole electric field [33] or to a negative charge depletion (or positive charge build up) associated with a slight further oxidation of the NpO_2. The latter phenomenon is often observed in semi-conductors, where the small concentration of charge carriers makes them susceptible to small additions of electron donors or acceptors [18]. NpO_2 is an intrinsic semiconductor with a well localized $5f^3$ impurity level. Further oxidation results in removal of electrons from this level thus explaining a Fermi energy decrease. The amount of additional oxygen is small because the Np-5f/O-2p intensity ratio only decreases from 0.36 in a to 0.32 in b.

With increasing oxygen dosage the surface further oxidizes (Fig. 5(A), c–e). The Np-5f level is further suppressed, showing the 5f count to decrease. This corresponds to an increased oxidation state (>+4) of the surface neptunium atoms. Neptunium shows a behaviour similar to uranium, where upon exposure to atomic oxygen, the 5f signal completely disappears, which was then attributed to the $5f^0$ configuration of U(VI) [9]. However, a quantitative estimate of the oxidation state based on the 5f absolute intensity for the neptunium is difficult, because we have no simple reference signal to which we can refer the absolute intensities (to correct for from measurement to measurement changed experimental parameters like surface reflectivity, lamp intensity, etc). The O-2p signal is not an ideal reference line because it increases itself upon oxidation. Just assuming unchanged experimental parameters, the area of the 5f emission for spectrum e (Fig. 5(A)) is reduced to 50% of the initial value (spectrum a), which would correspond to a reduction of the 5f count from $5f^3$ to $5f^{1.5}$, and an increase of the formal oxidation state from +4 to +5.5. The Np-5f/O-2p intensity ratio decreases to 0.129 (a decrease to 36%), which is also consistent with an Np oxidation state higher than +5.

Upon NpO_2 oxidation, the Np-5f line moves towards the O-2p line (Fig. 5(A), b–e). This movement superimposes with the shift of both lines to lower BE (Fermi level shift), but the O-2p line shifts stronger than the 5f line. The shift of the O-2p line is attributed to

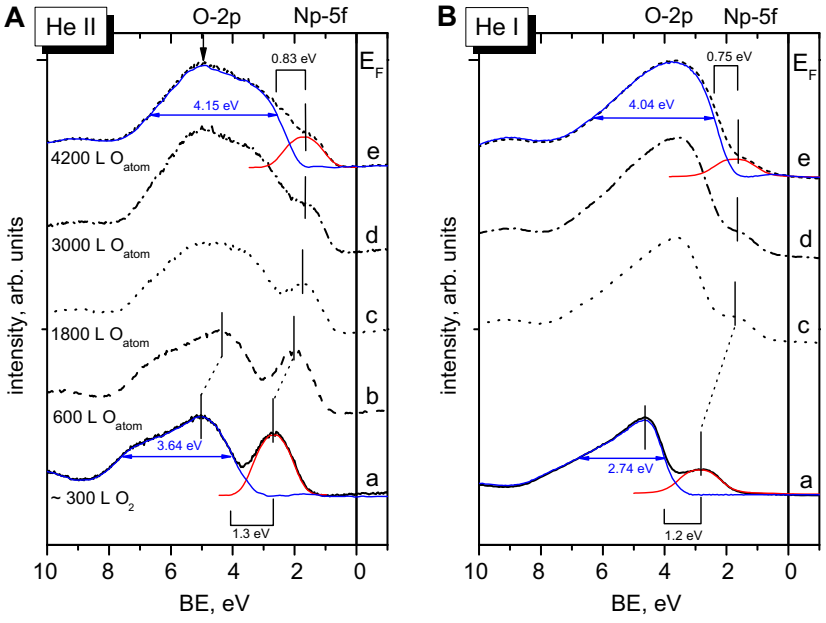

Fig. 5. UPS valence band spectra of NpO_2 film exposed to different dosages of atomic oxygen at room temperature. Graph A (left): HeII radiation (40.8 eV) was used; Graph B (right): HeI radiation (21.2 eV) was used. The vertical solid line represents the Fermi energy, E_F. Spectra represent the data for different O·dosages; (a): starting material $NpO_{2(-y)}$ (O_2 dosage of ~300 L on Np metal), (b–e): increasing dosage of O. Spectral shapes for Np-5f (red) and O-2p (blue) are given for spectra a and e. Marked in blue is the FWHM for the O-2p shapes. (For interpretation of the references to colour in this figure legend, the reader is referred to the web version of this article.)

the decrease of the Fermi energy (see above), because there is no reason to assume a chemical shift for the oxygen lattice atoms. After correcting for this rigid shift, the Np-5f lines even move to higher binding energy. This is interpreted as chemical shift, thus confirming Np oxidation.

Comparing HeII and HeI spectra (Fig. 5(A) and (B), respectively), further information can be obtained on the depth distribution and orbital type (p, d, f) of the species. HeII excited photoelectrons have an inelastic mean free path λ, of about one monolayer, thus probing the top surface, whereas the information depth for HeI is closer to that of the XPS core-level lines (Table 1). The cross-sections of the 5f states are enhanced by a factor of ~9 in HeII whereas the O-2p cross section decreases by a factor 1.5 (Table 1) [15]. HeII thus probes preferentially f states and the top surface region, HeI emphasises O-2p states and the bulk. Fig. 5 shows that for all oxygen dosages, the peak at ~2.8 eV is strongly suppressed in HeI (Fig. 5(B)), which corroborates its 5f character. Its decrease upon oxidation is less pronounced in HeI than in HeII: the Np-5f/O-2p area ratio decreases to 50% in HeI and 36% in HeII. Taking into consideration the deeper probing range of HeI, it is concluded that the oxidation is more pronounced at the top surface than below. Additional information on the top surface oxygen is provided by the shape of the O-2p peak. At high oxygen dosage, an additional intensity appears at the higher BE side of the O-2p peak. It appears as symmetrical peak at ~5 eV BE in HeII (arrow mark in Fig. 5(A)), but is missing in HeI. We attribute it to the O-2p level of chemisorbed oxygen, rather than lattice oxygen, because of the narrow shape and the high BE. Indeed, the narrow shape is characteristic of the narrow ground state of isolated atoms, in contrast to broad band peaks, associated with bulk atoms and the high BE is attributed to the decreased extra-atomic relaxation in adsorbed molecules compared to atoms embedded in a 3D lattice. A similar oxygen signal is observed on metallic Np at very low oxygen concentration (compare Fig. 1(A), 1 L spectrum) where it is also attributed to chemisorbed oxygen. Such chemisorbed oxygen bonds locally on surface Np atoms, thus leading to a higher local oxidation state, but it not necessarily forms a bulk compound. A similar observation was made for PuO_2 surfaces where, in spite of chemisorbed oxygen, no higher bulk oxide (PuO_{2+x}) was formed [9]. In contrast to this, no such peak is observed in bulk UO_3, where the O-2p signal shows a broadened, symmetric shape, but no high BE peak [9]. Finally there is also the possibility that the additional intensity ~5 eV is due to some f-character at the bottom of the O-2p band, which becomes pronounced in the HeII spectra due to the higher 5f cross-section of this excitation radiation. Band structure calculations are necessary to clarify this.

3.2.2. Core level data

Fig. 6 compares O-1s and Np-4f core level spectra of a NpO_2 film before and after exposure to atomic oxygen. Initially the O-1s peak is sharp with an asymmetrical tail at high BE, which can be associated either with chemisorbed surface oxygen or with extra lattice oxygen (e.g. bulk inhomogeneities). In fact, the HeII spectra indicate only very small amounts of extra surface oxygen, which could not explain alone the high BE component of the O-1s peak (corresponding to about one monolayer). Therefore this component is interpreted as lattice oxygen from bulk inhomogenieties.

After exposure the O-1s peak shifts to lower BE (~0.6 eV) and broadens significantly. Its FWHM increases from ~1.7 eV for NpO_2 to ~2.4 eV for the higher oxide. This broadening is not observed for the Np-4f spectrum, and thus typical for the O-1s line (no inhomogeneous charging). These observations point to the incorporation of extra oxygen forced into the lattice. A similar broadening is indeed observed for the O-2p level in UPS (see Fig. 5). The additional surface oxygen, shown by HeII, cannot explain this broadening alone, because it disappears already in the more bulk sensitive HeI excited spectrum, only a distinct broadening is observed as well. Recently an XRD study with a refined crystal structure for single crystals of Np_2O_5 showed that there are differently coordinated Np and oxygen sites [34], which would account for the broadened O-1s line. The O-1s shift to low BE corresponds to the outer level shifts observed in UPS and is attributed to the band bending in the near surface region, again associated with the incorporation of extra bulk oxygen.

For the Np-4f level no significant BE shift is detected (Fig. 6), but the high BE satellite of NpO_2 (at 6.7 eV higher BE) vanishes completely, after exposure to atomic oxygen. The absence of peak shift has to be interpreted as compensation of a shift to low BE (due to band bending) and a shift to high BE due to local oxidation of the Np atoms. The band bending shift, as estimated from the O-1s lines is of about 0.6 eV, therefore the chemical shift is also about 0.6 eV. Comparing these results to literature spectra and BE values for

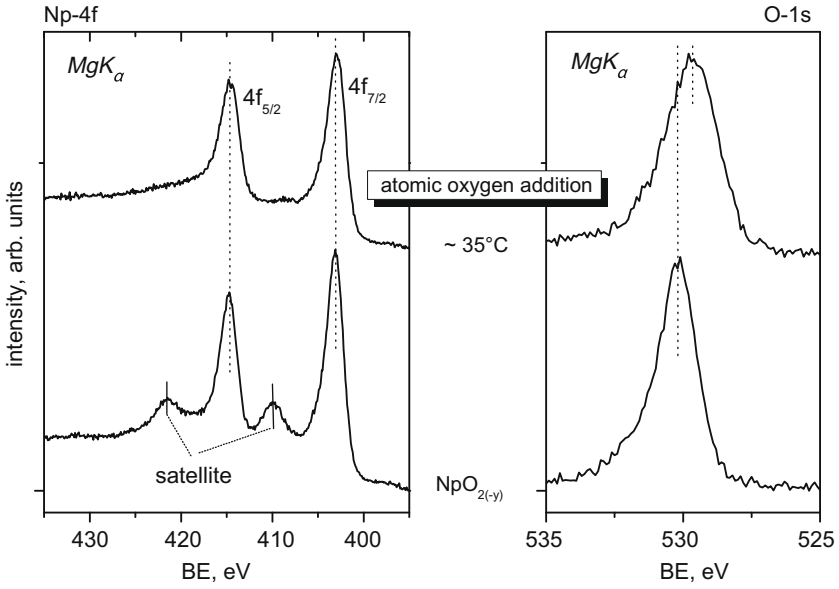

Fig. 6. XPS core level spectra (Np-4f and O-1s) of an originally $NpO_{2(-y)}$ film exposed to atomic oxygen at room temperature. Plotted spectra are not referenced. Mg K_α radiation (1253.6 eV) was used for XPS.

Np_2O_5 produced as bulk oxide by a completely different technique by Pan and Campbell [35] a good agreement is observed. Pan and Campbell found Np-4f BE values (C-1s referenced) for Np_2O_5 and NpO_2 that are comparable to our measurements (see Table 2). Again no Np-4f BE shift was observed and the 7 eV satellite disappeared in Np_2O_5. Unfortunately no O-1s BE data are given in [35]. As our in situ preparation does not allow referencing to the carbon contamination (because there is none) we can only give unreferenced BE values within a certain range (normally ±0.3 eV) for the different species as slight differences from specimen to specimen are observed. In conclusion, we identify our oxidation product as Np_2O_5. But the surface O/Np ratio, as deduced from the O-1s and Np-4f intensities, is higher than 2.5 expected for of Np_2O_5. Measured ratios vary between 2.6 and 2.9. This could be attributed either to the formation of a hyperstoichiometric oxide, Np_2O_{5+x}, under these drastic conditions (atomic O·), or additional chemisorbed oxygen may be present as proposed from the UPS data. The latter interpretation is corroborated by the presence of atomic oxygen O-2p signal, observed in the surface sensitive HeII spectra. Other chemisorbed oxygen species like hydroxylic groups, showing similar O-1s binding energies as that found for the shoulder in our spectra (~531 eV [19,36]), can be ruled out because their characteristic UPS emissions are missing. If only the main (oxidic) peak for O-1s is taken into account for the calculation of the O/Np ratios, values around 2.5 were obtained (the area of the fitted shoulder varied between 7% and 12% of the total peak area). The ability of Np_2O_5 to chemisorb oxygen atoms must be due to the remaining 5f states which, in spite of being localized, preserve a bonding capability (dangling bonds). A similar behaviour was observed for the 5f state in PuO_2 [9].

3.3. Thermal stability of the oxidised species

The oxide films discussed so far develop as thin surface layers on metal systems of about 100 atomic layers. They are heterogeneous because at room temperature, diffusion processes are slow. As consequence, complex bulk systems with different oxidation states coexist with surface systems and chemisorbed oxygen. To obtain more homogeneous samples and to assess their thermal stability, heating was applied. Heating has two possible effects: it enhances bulk diffusion processes, but as well may trigger surface decomposition (oxygen released into vacuum chamber). To distinguish these reaction routes two different heating experiments are carried out. First the samples are heated in absence of oxygen, to determine their range of thermal stability. Then heating is done under atomic oxygen atmosphere, to allow the films reaching their stable end composition under oxygen saturation and solid state mobility (oxygen can diffuse into the deeper layers saturating the entire film).

Fig. 7 shows the vacuum heating of a NpO_{2+x} film, produced at ~25 °C by exposing NpO_2 to atomic oxygen. The temperature was gradually raised up to 300 °C, and the surface evolution monitored by HeII and HeI spectroscopies. With increasing temperature the O-2p band narrows and develops a shape similar to that in NpO_2. The Np-5f peak increases in intensity and the entire spectrum shifts to higher BE. All these features constitute a reversal of the effect of oxygen addition (see Section 3.2.1) and are thus characteristic for the reduction of NpO_{2+x} into NpO_2. At 250 °C this process is complete. When the temperature is further increased to 300 °C, a new peak appears at the low BE side of the Np-5f line (Fig. 7(A), arrow mark). It has a BE characteristic for Np_2O_3 (compare Fig. 1(A)), and is more pronounced in surface sensitive HeII than in HeI: the top surface is more reduced than the underlying bulk, proving again that the trivalent character for neptunium (in Np_2O_3) distinctly appears in the surface layers.

It is not clear at that point whether the oxygen loss upon heating is due to oxygen diffusion into the bulk (reacting with reduced deeper layers or the substrate), or whether oxygen is just released from the surface layer into the vacuum because of the thermal instability of the higher oxide. To answer this question, we exposed the surface to large dosages of O· at increasing temperature. If the oxide is unstable, it should not form again. But if the decomposition was due to bulk diffusion of oxygen, then the entire film should eventually become saturated under conditions, where diffusion is thermally allowed and a saturation oxygen dosage added. For UO_2 it was indeed shown that UO_3 bulk oxide could be produced in this way and was stable at elevated temperatures, while PuO_2 did not further oxidize [9]. Fig. 8 shows the corresponding data set for NpO_2, for temperatures ranging from ~30 to 400 °C. Valence band (HeII) and Np-4f (XPS) data are given. The room temperature HeII spectrum shows two prominent features, the

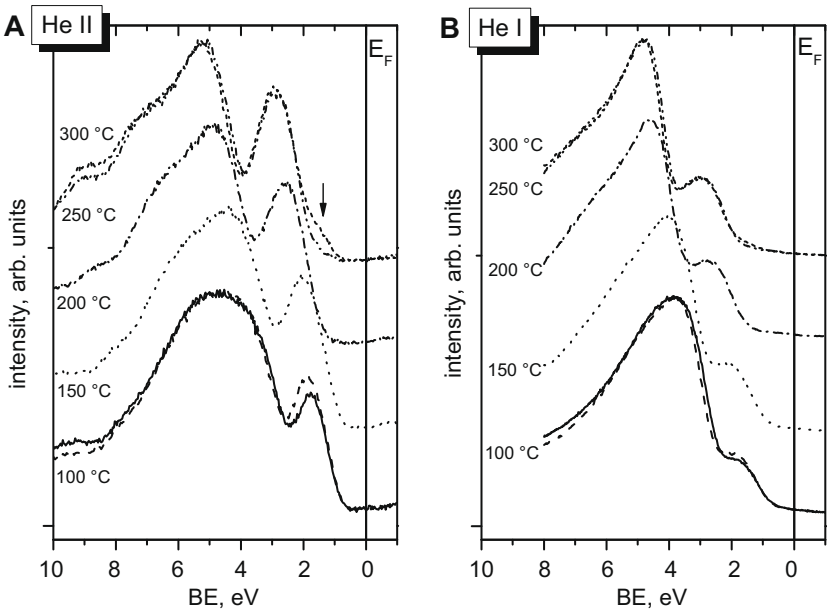

Fig. 7. UPS valence band spectra of NpO_2 film exposed to atomic oxygen at 25 °C (solid curve) and heated to various temperatures up to 300 °C without additional exposure. The solid vertical line represents the Fermi energy, E_F. Temperatures are measured at the substrate holder. A: HeII radiation (40.8 eV), B: HeI radiation (21.2 eV) used for UPS.

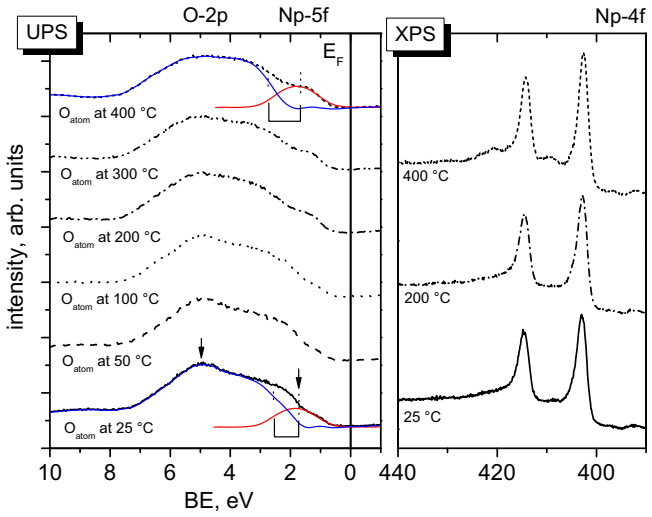

Fig. 8. UPS valence band and XPS Np-4f core level spectra of NpO_2 film exposed to atomic oxygen at RT (~25 °C) and various $T \leqslant 400$ °C. Temperatures are measured at the substrate holder. The solid line represents the Fermi energy, E_F. Arrow marks are explained in the text. HeII radiation (40.8 eV) was used for UPS, Mg K_α excitation radiation (1253.6 eV) for XPS.

reduced 5f peak at ~1.7 eV BE and the O-2p peak of chemisorbed oxygen at ~5 eV (arrow marks in Fig. 8). When the temperature is raised, both features are remarkably stable at least till 200 °C. When heating without oxygen (Fig. 7) the chemisorbed oxygen signal disappeared at this temperature, and the Np-5f intensity increased to the value in NpO_2. Bulk diffusion is thus responsible for NpO_{2+x} decomposition below 200 °C and exposing the surface under these conditions to atomic oxygen simply replaces the oxygen loss.

At 300 °C and 400 °C, the signal of chemisorbed oxygen is suppressed but the Np-5f peak is still small – there is no sign for reappearing NpO_2. The only sign for slight reduction is the ongoing separation of the Np-5f and the O-2p emission at 400 °C, where the O-2p level shifts to higher BE away from the Np-5f peak. This may be interpreted as increase of the Fermi-energy, i.e. surface reduction, together with a decrease of the Np-5f BE, again a signal for Np reduction. But the reduction at the top surface is not very pronounced, as seen by the virtually unchanged 5f intensity.

Np-4f spectra corroborate the valence band data. Up to 200 °C no significant differences in the Np-4f core level (right graph in Fig. 8) are observed. The spectra are characteristic for Np_2O_5. But above 200 °C the 7 eV satellite, characteristic of NpO_2, appears again showing a decomposition of the higher oxide (upper most spectrum in Fig. 8, measured on 400 °C sample).

4. Summary and conclusions

Molecular O_2 reacts readily with the metallic neptunium surface to form the sesquioxide and dioxide. The sesquioxide is observed as thin 'bulk' species of several monolayers thickness, which forms as long as the metal is present. Up to now it was only reported as surface phase. Our findings show that the reactivity of neptunium is intermediate between uranium and plutonium: while U does not form a sesquioxide, from Pu on the sesquioxide exists as stable bulk phase.

A higher oxide, Np_2O_5, is formed when the NpO_2 surface is exposed to atomic oxygen. Under similar reaction conditions uranium oxidizes to UO_3 whereas plutonium does not oxidize beyond PuO_2 and additional oxygen is only chemisorbed on the outermost surface. The higher Np oxide is characterized by a reduced Np-5f signal compared to NpO_2 and the absence of shake-up satellites in the Np-4f core-level spectrum. It is stable under UHV conditions up to a temperature of about 200 °C.

The higher oxide, Np_2O_5, is still capable to chemisorb further oxygen. This is shown in UPS spectra by the additional O-2p line at 5-6 eV BE, superimposing onto the valence band. Such local bonds are a sign for the residual bonding power of the localized 5f states of Np^{5+}. This is as well consistent with the trend throughout the actinide series, where for the higher oxide of plutonium (PuO_2) a similar behaviour is found but not for the uranium trioxide (with no occupied 5f states) [9].

Formation of both lower and higher oxide (Np_2O_3 and Np_2O_5, respectively) besides the dioxide can be accounted to one explanation: the increasing localization of the 5f states due to orbital contraction with increasing atomic number, Z. The ability of these states to contribute to bonding thus decreases. On the one hand this explains the stability of the lower oxide Np_2O_3, which involves only the three ds valence electrons, while the 5f states are non-bonding (in UPS, they are shifted away from the Fermi-level). On the other hand, it accounts for the higher oxide Np_2O_5 (with Np^{5+}), which is lower than the highest oxide for uranium (UO_3 with U^{6+}) but is not observed for plutonium (PuO_2 with Pu^{4+}) under similar conditions.

Acknowledgements

A.S. acknowledges the European Commission for support given in the frame of the program 'Training and Mobility of Researchers'. The high purity Np metal required for the production of the thin film compounds was made available through a loan agreement between Lawrence Livermore National Laboratory and ITU, in the frame of a collaboration involving LLNL, Los Alamos National Laboratory, and the US Department of Energy.

References

[1] J. Bruno, R.C. Ewing, Elements 2 (2006) 343.
[2] Th. Fanghänel, V. Neck, Pure Appl. Chem. 74 (2002) 1895.
[3] H.M. Haschke, T.H. Allen, L.A. Morales, Science 287 (2000) 285.
[4] M.S. Coonley (Ed.), Los Alamos National Laboratory, Actinide Research Quarterly, second quarter, 2004.
[5] P. Martin, S. Grandjean, M. Ripert, M. Freyss, P. Blanc, Th. Petit, J. Nucl. Mater. 320 (2003) 138.
[6] P.A. Korzhaviy, L. Vitos, D.A. Andersson, B. Johansson, Nat. Mater. 3 (2004) 225.
[7] V. Neck, M. Altmaier, Th. Fanghänel, J. Alloys Compd. 444&445 (2007) 464.
[8] D.L. Clark, S.S. Hecker, G.D. Jarvinen, M.P. Neu, Neptunium, in: L. Morss, N.M. Edelstein, J. Fuger (Eds.), The Chemistry of the Actinide and Transactinide Elements, vol. 2, Springer, Dordrecht, 2006, p. 813.
[9] T. Gouder, A. Seibert, L. Havela, J. Rebizant, Surf. Sci. 601 (2007) L77.
[10] C.A. Colmenares, Prog. Solid State Chem. 15 (1984) 257.
[11] D.T. Larson, J. Vac. Sci. Technol. 17 (1980) 55.
[12] R.G. Haire, J. Alloys Compd. 223 (1995) 185.
[13] D.M. Gruen, W.C. Koehler, J.J. Katz, J. Am. Chem. Soc. 73 (1951) 1475.
[14] M.P. Seah, W.A. Dench, Surf. Interface Anal. 1 (1979) 2.
[15] J.J. Yeh, I. Lindau, Atom. Data Nucl. Data Tables 32 (1985) 1.
[16] S. Doniach, M. Sunjic, J. Phys. C 3 (1970) 285.
[17] J.R. Naegele, J. Ghijsen, Localisation and hybridisation of 5f states in the metallic and ionic bond as investigated by photoelectron spectroscopy, in: L. Manes (Ed.), Actinides – Chemistry and Physical Properties Structure and Bonding, vol. 59/60, Springer-Verlag, Berlin, 1985, p. 197.
[18] A. Zangwill, Physics at Surfaces, 1st Ed., University, Cambridge, 1988.
[19] K. Wandelt, Surf. Sci. Reports 2 (1982) 1.
[20] R. Naegele, L.E. Cox, J.W. Ward, Inorg. Chim. Acta 139 (1987) 327.
[21] P.S. Bagus, F. Illas, G. Pacchioni, F. Parmigiani, J. Electron. Spectrosc. Related Phenom. 100 (1999) 215.
[22] I. Lindgren, J. Electron. Spectrosc. Related. Phenom. 137–140 (2004) 59.
[23] B.W. Veal, D.J. Lam, H. Diamond, H.R. Hoekstra, Phys. Rev. B 15 (1977) 2929.
[24] N. Beatham, A.F. Orchard, G. Thornton, J. Electron. Spectrosc. Related. Phenom. 19 (1980) 205.
[25] J. Weber, V.A. Gubanov, J. Inorg. Nucl. Chem. 41 (1979) 693.
[26] Y. Baer, J. Schoenes, Solid State Commun. 33 (1980) 885.
[27] L.E. Cox, W.P. Ellis, R.D. Cowan, J.W. Allen, S.-J. Oh, Phys. Rev B (1985) 2467.
[28] J.J. Pireaux, J. Riga, E. Thibaut, C. Tenret-Noel, R. Caudano, J.J. Verbist, Chem. Phys. 22 (1977) 113.
[29] E.S. Ilton, P.S. Bagus, Surf. Sci. 602 (2008) 1114.

[30] W.-D. Schneider, C. Laubschat, Phys. Rev. Lett. 46 (1981) 1023.
[31] O. Gunnarsson, D.D. Sarma, F.U. Hillebrecht, K. Schönhammer, J. Appl. Phys. 63 (1988) 3676.
[32] M.P. Seah, Quantification of AES and XPS, in: D. Briggs, M.P. Seah (Eds.), Practical Surface Analysis, vol. 1, John Wiley, Chichester, 1990, p. 201.
[33] M. Batzill, U. Diebold, Prog. Surf. Sci. 79 (2005) 47.
[34] T.Z. Forbes, P.C. Burns, S. Skanthakhumar, L. Soderholm, J. Am. Chem. Soc. 129 (2007) 2760.
[35] P. Pan, A.B. Campbell, Radiochim. Acta 81 (1998) 73.
[36] J.D. Farr, R.K. Schulze, M.P. Neu, J. Nucl. Mater. 328 (2004) 124.